Wall Shear Stress Distribution of non-Newtonian Blood Flow in Stenosed Bifurcated Artery

[1]Norliza Mohd Zain, [2]Muhammad Sabaruddin Ahmad Jamali, [1]Zuhaila Ismail* and [1]Lim Yeou Jiann

[1]Department of Mathematical Sciences, Faculty of Science, Universiti Teknologi Malaysia
81310 UTM Johor Bahru, Johor, Malaysia

[2]School of Mechanical Engineering, College of Engineering, Universiti Teknologi MARA
40450 Shah Alam, Selangor, Malaysia

*Corresponding author: zuhaila@utm.my

Abstract Localized plaque causes narrowing of the arterial wall, resulting in an alteration in the flow structure, reducing the flow of fluids reaching the heart and resulting in heart attacks. The formation of stenosis could disturb the normal hemodynamics in blood rheology. A bifurcated artery with different types of stenosis is considered in order to illustrate the four possible formations of plaque between healthy and diseased arteries. Due to the fact that a diseased artery is reported to be less compliant, the artery wall is modelled as a two-dimensional rigid wall. In this model, blood flow is assumed to be steady, laminar, incompressible, and characterized as a generalized power-law model that is non-Newtonian in nature. The numerical simulation is performed using COMSOL Multiphysics, which is based on finite element method. Based on simulation results, different types of stenosis in the bifurcated artery have a significant impact on velocity profiles and wall shear stresses.

Keywords Bifurcated artery; COMSOL; non-Newtonian; Stenosis; Wall shear stress.

Mathematics Subject Classification 75D05; 76-04.

1 Introduction

Cardiovascular disease related to coronary artery disease is typically caused by atherosclerosis, formed when cellular waste products, fatty substances, smooth muscle cells and cholesterol accumulate in the arterial lumen [1,2]. The localization of plaque, which in medical terms is known as stenosis, leads to a reduction in arterial passage area that considerably disturbs the normal blood circulation to the other organs and tissues [3,4]. Plaque ruptures may occur as the condition worsens, exposing an individual to severe cardiovascular diseases and eventually leading to a stroke or heart attack. It has been demonstrated that the geometry of the bifurcated artery can be classified according to the angle between the mother and daughter arteries and the location of plaque formation. When the angulation is greater than (>) 70°, the T-shaped branch artery is obtained where the shifting to

the branch is slightly complicated in comparison to Y- shaped branch artery with angle between the mother and daughter artery less than (<) 70° [5]. In this work, four different types of model have been considered according to [5-8] to investigate the distribution of plaque formation for anatomic considerations. Until now, the adoption of coronary treatment by using stent have always been a major challenge especially for bifurcation case. Stents were conventionally used in clinical practice for the treating cardiovascular diseases until endovascular therapies were developed. The stent restores the flow of blood in a disease vessel and helps to reduce the chance of a heart attack depending on where it is placed. Knowledge of stent implantation in bifurcated artery is crucial for the understanding on the changes of the arterial blood flow pattern and the distribution of wall shear stress. The study of stent implantation using an in vitro pulse duplication system has been conducted by Peacock *et al.* [9]. The result in vivo and vitro studies has concluded that the flow patterns are globally and locally affected by the stent structure [10]. Using a three-dimensional model of healthy and stented coronary artery bifurcation, Zarandi *et al.* [11] investigated non-Newtonian hemodynamics and shear stress distribution. The flow behaviours and shear stress profiles near the arterial wall in stented coronary artery were discovered to induce the local flow disturbance where the lowest value of wall shear stress were developed at the intra-stent region of the mother and daughter arteries.

A Newtonian model of blood rheology can be applied to fluid flowing through large arteries with shear rates exceeding 100 s^{-1} (reciprocal seconds) [12,13]. However, for fluid flows through a diseased vessel that possessed an arterial constriction, the hemodynamical behaviours of fluid in this network of vessels exhibits the hemodynamics property which accurately described as a non-Newtonian model [14]. Johnston *et al.* [15] explored the significance of an accurate consideration of blood rheological representation by considering both Newtonian and few other non-Newtonian blood rheological models comprised of the Walburn-Schneck model, Carreau model, power law model, generalized power law model as well as the Casson model, in treating the blood flow characteristics. They discovered that for a high inlet velocity, the distributions of wall shear stress between the Newtonian and non-Newtonian model are similar. Whereas, when the inlet velocity is lower, they obtained low wall shear stress values for Newtonian model in comparison to the other non-Newtonian models. They also found that the distributions of shear stress exerted on the wall for the Power Law and Walburn-Schneck models were underestimated in comparison to the other types of rheological model. In comparing the Newtonian model to the generalized power law model, Johnston *et al.* [16] conclude that the wall shear stress is approximated at a relatively small value for low inlet velocities at low shear regions. Johnston *et al.* [16] examined five different non-Newtonian models of coronary blood flow in the right coronary arteries. It is kind of impossible to capture a single constitutive relation in predicting all of the non-Newtonian behaviours of the fluid flowing in various situations [17]. From various non-Newtonian models, the generalized power law model is chosen here to represent the rheological behaviours of blood due to its combination property of a Newtonian model at a low shear rate, the power law model at a high shear rate and the Casson model as a special case [17]. Further, Bakheet *et al.* [18] have also recommended the use of a generalized power law model during the low inlet velocities and low shear rates flow to gain an excellent estimation of shear stress along the arterial's wall. The influence of the shape of stenosis on the blood flow behaviours has been investigated in [19] by considering the rheological behaviours of blood as the generalized power law model. The shear-thinning as well as shear-thickening natures of non-Newtonian fluid has been successfully examined in [20] by characterising the fluid's behaviour as a generalized power law fluid model which passes through an artery with differently shaped constrictions. The implications

of different stages of atherosclerotic disease development to blood haemodynamics that is treated as a generalized power law fluid was examined in [21] by considering a mild shaped constriction with 48%, 64% and 84% cross-sectional area of reduction.

Motivated by the findings from the cited studies, focus will be made on the effect of stenosis located at various locations in a branch artery by considering the blood as a laminar flow that is treated as a generalized power law model. The simulations carried out in this study are obtained by using a computational software which works according to the finite element algorithms, known as Comsol Multiphysics 5.2.

2 Mathematical Formulation

Prior to the formulation of the mathematical model, a few assumptions are imposed on the computational domain of branch artery that possess a stenosis. These include:

1. The branch artery is of finite length.

2. The consideration of four types of morphology with different stenosis formation consist of Type I to Type IV.

3. At the lateral junctions and on the flow divider of the branch artery, curvatures are introduced so that discontinuities causing nonexistent separation zones can be eliminated.

The atherosclerotic lesions are portrayed by using several kinds of classification which describes the formation of stenosis as proposed in [9-12]. In this work, two models of a bifurcation are added (TYPE I and TYPE III) to display the four possible types of morphology as shown in Figure 1. A healthy artery is referred as TYPE I. Stenosis of parent arteries proximal to bifurcations is classified as TYPE II. Stenosis located in the parent artery which goes further into the upper wall of bifurcation is categorized as TYPE III. Stenosis of TYPE IV occurs in the parent vessel, near the ostium of the bifurcation, and proximal to the bifurcation.

Let us consider the incompressible flow of generalized power law model through a stenosed bifurcated artery with 4 different morphologies where the flow is assumed to be steady and laminar. Hence, the suitable two-dimensional governing equations for such fluid flow are governed in non-dimensional form by these following equations, stated as

$$\frac{\partial u}{\partial x} + \frac{\partial v}{\partial y} = 0, \tag{1}$$

$$\left[u\frac{\partial u}{\partial x} + v\frac{\partial u}{\partial y} \right] = -\frac{\partial p}{\partial x} + \frac{1}{Re}\left(\frac{\partial \tau_{xx}}{\partial x} + \frac{\partial \tau_{xy}}{\partial y} \right), \tag{2}$$

$$\left[u\frac{\partial v}{\partial x} + v\frac{\partial v}{\partial y} \right] = -\frac{\partial p}{\partial y} + \frac{1}{Re}\left(\frac{\partial \tau_{xy}}{\partial x} + \frac{\partial \tau_{yy}}{\partial y} \right), \tag{3}$$

where,

$$\bar{\tau} = -\left\{ m\left| \sqrt{\frac{1}{2}\left(\underline{\Delta} : \underline{\Delta} \right)} \right|^{n-1} \right\} \underline{\Delta}, \tau_{xx} = -2\left\{ m\left| \left[\frac{1}{2}\left(\underline{\Delta} : \underline{\Delta} \right) \right]^{1/2} \right|^{n-1} \right\}\left(\frac{\partial u}{\partial x} \right),$$

$$\tau_{yy} = -2\left\{m\left\|\left[\frac{1}{2}(\underline{\Delta}:\underline{\Delta})\right]^{1/2}\right\|^{n-1}\right\}\left(\frac{\partial u}{\partial y}\right),$$

$$\tau_{xy} = \tau_{yx} = -\left\{m\left\|\left[\frac{1}{2}(\underline{\Delta}:\underline{\Delta})\right]^{1/2}\right\|^{n-1}\right\}\left(\frac{\partial v}{\partial x}+\frac{\partial u}{\partial y}\right), \underline{\Delta}_{ij} = \left(\frac{\partial v_i}{\partial x_j}\right)+\left(\frac{\partial v_j}{\partial x_i}\right), \text{ and}$$

$$\frac{1}{2}(\underline{\Delta}:\underline{\Delta}) = 2\left[\left(\frac{\partial u}{\partial x}\right)^2+\left(\frac{\partial v}{\partial y}\right)^2\right]+\left[\frac{\partial v}{\partial x}+\frac{\partial u}{\partial y}\right]^2-\frac{2}{3}\left[\frac{\partial u}{\partial x}+\frac{\partial v}{\partial y}\right]^2.$$

The parameters i and j represent the respective values of x and y. While, the parameter $\underline{\Delta}$ in Equation (3) refers as the symmetrical rate of deformation tensor. The dimensionless parameter of Reynolds number, Re is obtained as

$$Re = \frac{\rho u_\infty L}{\mu}.$$

$\bar{\tau}$ denotes the stress tensor, u is the velocity in x-direction, v is the velocity in y-direction. The axial and radial coordinates are characterised in two-dimensional Cartesian coordinate system as x and y, respectively. Parameters such as the dynamic viscosity of blood, density of blood, and pressure distribution on the surface are represented by μ, ρ and p,respectively. The shear forces exerted along the arterial wall is calculated using the expression defined as,

$$\tau = \mu\left(\frac{\partial v}{\partial x}+\frac{\partial u}{\partial y}\right),$$

based on the findings obtained for the axial and radial flow velocity.

To solve the governing equations specified in Eqs. (1)–(3), the appropriate governing equations are imposed along the boundary of the bifurcated artery. The inlet of the artery is imposed with a parabolic velocity profile, $u(x, y)$ as shown in the equation below

$$u(x,y) = u_{\max}\left(1-\left(\frac{y}{a}\right)^{\frac{n+1}{n}}\right) \text{ and } v(x,y) = 0, \text{ at } x = 0, \text{ and } -a \le y \le a. \qquad (4)$$

Meanwhile, the no-slip conditions are prescribed along all the wall of the branch artery

$$u(x,y) = 0, \ v(x,y) = 0. \qquad (5)$$

A traction-free configuration is employed at the branch artery outlet, which can be described as follows

$$(-p\mathbf{I}+\tau)\cdot\mathbf{n} = 0, \qquad (6)$$

where a unit for the outward normal vector is characterized as **n**. At the axial and radial coordinate of $(x, y) = (0, 0.5)$, a pressure point constraint, $p(x, y) = 0$ is being employed.

3 Numerical Results and Discussion

A different type of blood rheology was investigated numerically by calculating the axial velocities at the mother and daughter arteries as well as visualizing the streamlines and wall shear stresses. The specific location where the evaluation of the flow variables for all TYPE of the geometrical model

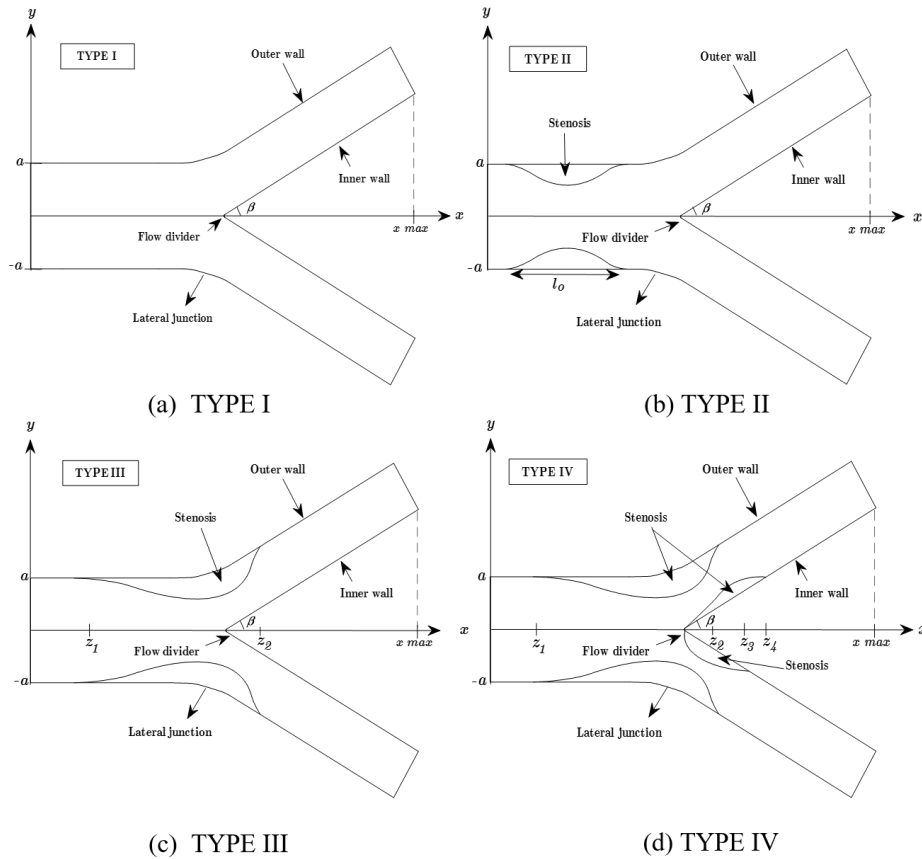(a) TYPE I

(b) TYPE II

(c) TYPE III

(d) TYPE IV

Figure 1: Geometry of Bifurcated Artery with Various Kinds of Morphologies: (a) TYPE I, (b) TYPE II, (c) TYPE III, (d) TYPE IV

are labelled as shown in Figure 2. Velocity profiles of generalized power law model simulations are studied for three different lines inside the bifurcated artery. The first line, denoted as L1, is located right before the main bifurcation, the second line, L2, is at the upper bifurcation, and the last line, L3, located at the lower bifurcation.

3.1 Velocity Profile for Different TYPE of Model

The cross-sectional profiles of the axial velocity corresponding to different axial position and value of generalized power law index, n which describes the flow with varying vicosity of blood for Re = 300 are illustrated in Figure 3 to Figure 5. Based on the figures shown, it is clearly seen that the magnitudes for the velocity of blood are gradually decreased from the respectives maxima to zero velocity at the wall. The distributions of velocity obtained here are correspond to the no-slip boundary condition prescribed at the wall and the assumption that the vessel behaves like a rigid tube. From the outcome, it seems that the velocity becomes significantly higher for TYPE III and TYPE IV which is contributed by the narrowing of an artery. Meanwhile TYPE I in Figures 3(a), 3(b) and 3(c) shows the normal parabolic velocity profile without the backflow occurrence since there are no constricted area at these locations. However, TYPE II in Figures 3(b) and 3(c) show that the backflow and flow separation has occurred at the wall of the artery as the velocity values are found negative here. The transitions of blood rheological behaviour from shear-thinning (n=0.639) to Newtonian (n=1) and then to shear-thickening (n=1.2) fluid models happened as the generalized power law index, n are
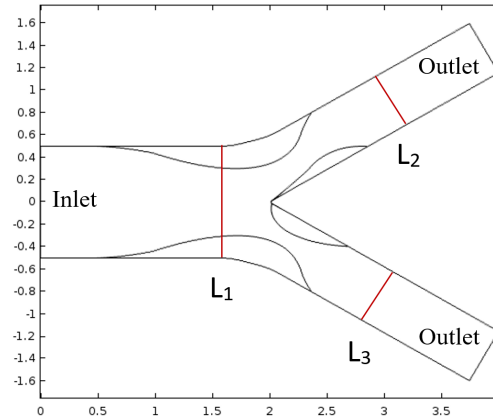
Figure 2: Location for Evaluation of Problem Variables for All TYPE of Geometry

increased (refer to Figures 3(a), 3(b) and 3(c)). Interesting to note that the magnitude of the velocity for Figure 3(c) are higher to those 3(a) and 3(b).

Figure 4 illustrated the velocity profile in upper bifurcated artery part at location (L_2) for different rheology of blood. A no-slip condition and the assumption that the vessel behaves like a rigid tube result in zero velocity at both sides of the wall. There is a skewed velocity profile for TYPE I, TYPE II, and TYPE III along the line (L2), which refers to the inner wall of the daughter artery in this case. The flow is much faster at this side in comparison to the other side as the maximum velocity is achieved here. In contrast, velocity profile for TYPE IV is skewed to the left and possessed the highest value compared to those in TYPE I, TYPE II and TYPE III. The findings obtained for Newtonian and shear-thickening fluid models also show that the velocity profiles for TYPE III and TYPE IV are declined to the negative value after reaching zero which indicates that the recirculation areas are formed near the arterial wall. In Figure 3, the magnitude of maximum velocity for all types of constricted geometry except for TYPE IV is lower than that at the location (L1) due to part of the flow already decelerating after becoming obstructed in the mother artery and flow divider. Meanwhile, TYPE IV exhibit highest velocity magnitude at (L_2) as compared to (L_1) since TYPE IV consist of stenosis at the outer and inner wall of upper bifurcate. Hence, the high velocity fluid layer were forced to move more slowly as it passes the constricted region.
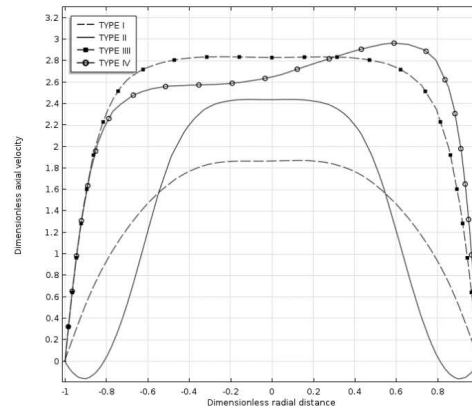
Figure 5 illustrated the velocity profile formed in lower bifurcated artery at location (L_3) for different rheology of blood. Assuming the vessel behaves like a rigid tube, velocity is zero at both sides of the wall in all cases. Noticed here as well is the profiles pattern for the axial velocity along the line (L_3) which distributed in a similar pattern as the profiles of velocity along the line (L_2) for all TYPE cases as found in Figure 4. Moreover, the magnitudes of maximum velocity for all TYPE are observed to be lower than those obtained at the (L_1) location as indicated in Figure 3, due to the flow disturbance that has occurred at the mother artery as well as along the flow divider which contributes to a decelerated flow. As the generalized power law index n increases, the maximum velocity magnitude for all TYPE gets higher. However, TYPE IV exhibit lowest magnitude of velocity compared to those in 5(a) but highest in 5(c). Velocity TYPE I and TYPE II shows no negative value for all different values of n. Velocity for TYPE III shows the negative value after reaching zero for $n=1$ and $n=0.639$ due to the formation of flow reversal along the outer arterial wall of the branch artery. The flow velocity for TYPE IV has been considerably affected by a more complex and severe type of stenosis indicated by the negative flow formed in the vicinity of the outer arterial wall for all values of n.
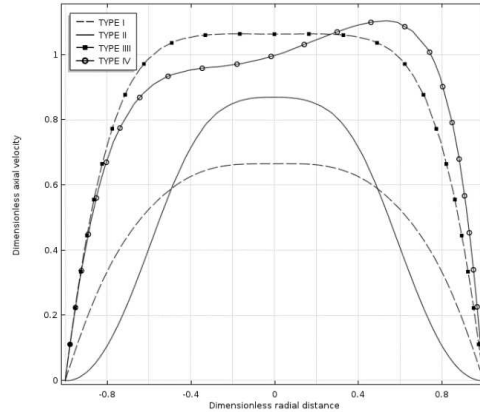
(a)
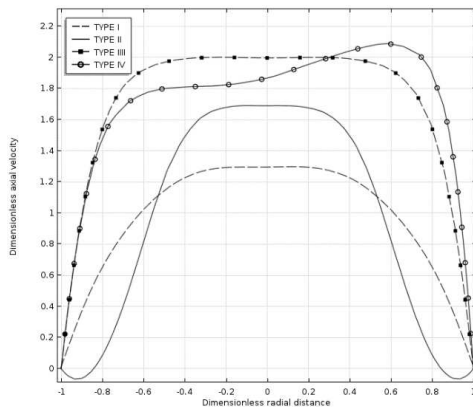
(b)   (c)

Figure 3: Velocity Profile at Location L_1 for (a) n=0.639, (b) n=1, (c) n=1.2

Figure 6 illustrated the velocity profile in the most diseased artery, TYPE IV, for different type of blood rheology. Clearly observed in Figure 6(a) and 6(b) that the shear-thickening model has attained the greatest magnitudes of velocity. From Figure 6(b), there is a skewed velocity profile in the upper and lower bifurcated arteries, with the maximum velocity occurring at the other ends. One can observe that the velocity in upper bifurcate is higher as compared to those found in the lower bifurcate. However, the velocity for shear-thickening model shows the highest in upper and lower bifurcated artery as compared to those Newtonian and shear-thinning models. Due to the slight differences in shape and size of the stenosis in upper and lower bifurcated arteries, hence this will give a considerable impact on the flow pattern and velocity along this region.

3.2 Wall Shear Stress Distribution

For four different types of bifurcated arteries, Figure 7 displays the wall shear stress distributions along the bifurcated artery for Newtonian rheological behaviour (n=1), shear-thinning rheological behaviour (n=0.639), and shear-thickening rheological beha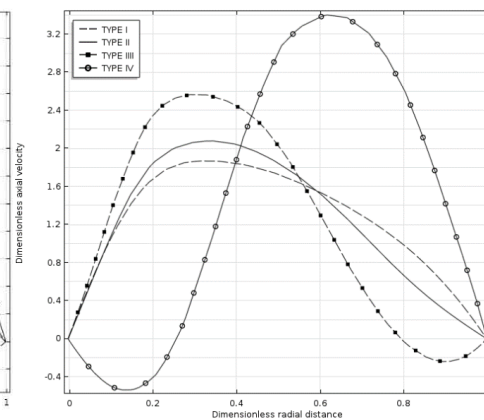viour (n=1.2) by using Re=300. As can be seen from this figure, the shear-thickening model has the highest shear stress value
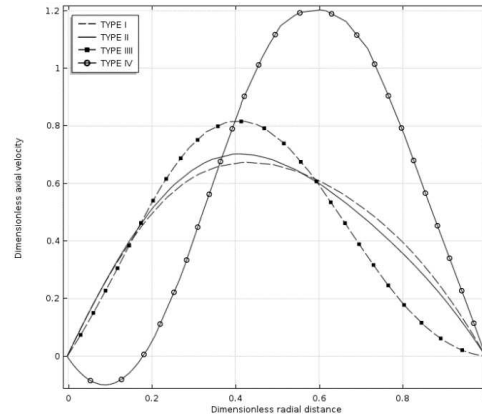
(a)
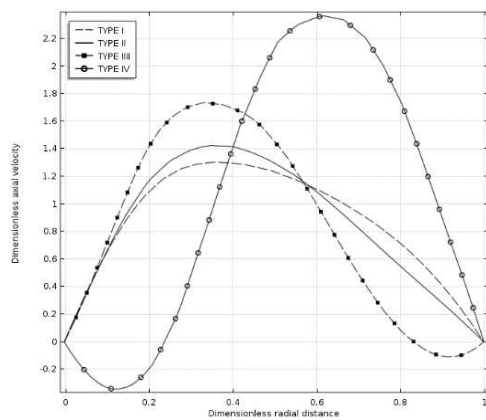
(b)

(c)

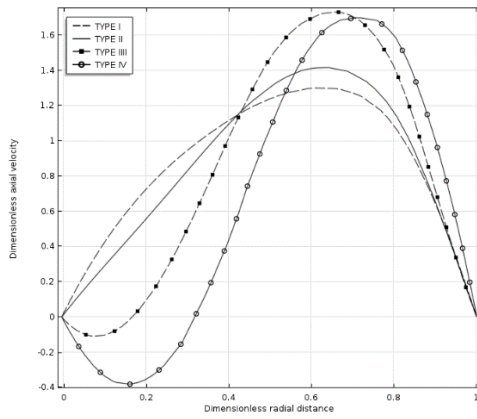Figure 4: Velocity Profile at Location L_2 for (a) n=0.639, (b) n=1, (c) n=1.2

exerted on the wall. The peak of the wall shear stress corresponds to the narrowest points of the cross-section (TYPE II- TYPE IV), while the peak of wall shear stress for TYPE I corresponds to the lateral junction of bifurcated artery. A profile of wall shear stress illustrates stenosis geometry in which upstream of the stenosis, the wall stress increases rapidly until it reaches the stenosis throat. At the critical height of the stenosis, wall shear stresses reach their maximum and then decrease downstream. As the shear stress exerted on the wall attains a negative value, this indicating that the flow reversal is occurred at that region. The occurrence of flow reversal is presented in TYPE II, TYPE III, and TYPE IV cases for the shear-thinning, Newtonian and shear-thickening models. According to Yao *et al.* [22], the wall shear stress distribution contributes significantly to the discovery of platelet aggregation sites. Shear forces in the wall could be amplified at stenotic area, contributing to its rupture, leading to paralysis in the affected region.
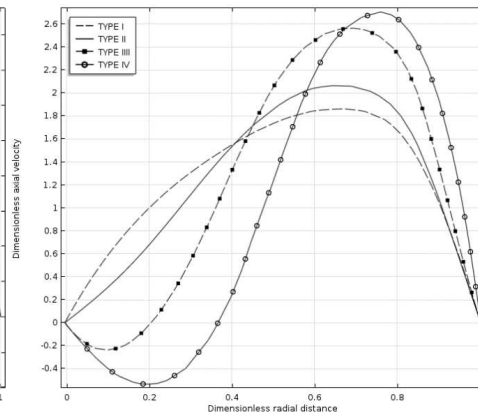
4 Conclusion

The non-Newtonian model of blood flow has been successfully characterized as a generalized power law model by analyzing steady, laminar and incompressible fluid flows in a branch artery with four types of morphologies related to stenosis location. Based on the different morphologies considered,
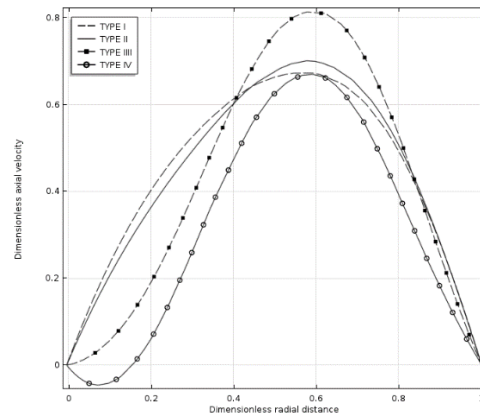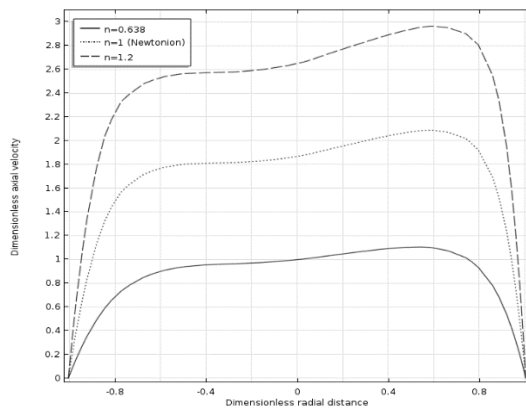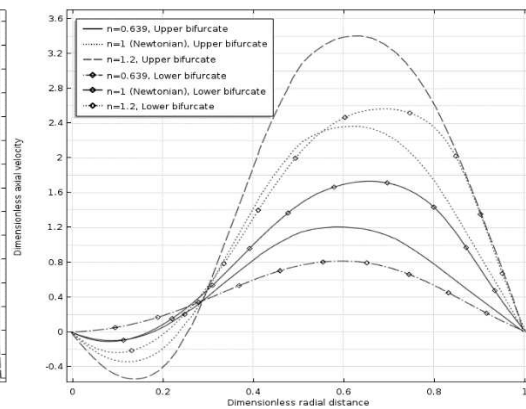
(a)

(b)   (c)

Figure 5: Velocity Profile at Location L$_3$ for (a) *n*=0.639, (b) *n*=1, (c) *n*=1.2

(a)   (b)

Figure 6: Velocity Profile for TYPE IV with Different blood rheology at (a) mother artery, and (b) daughter artery

(a)

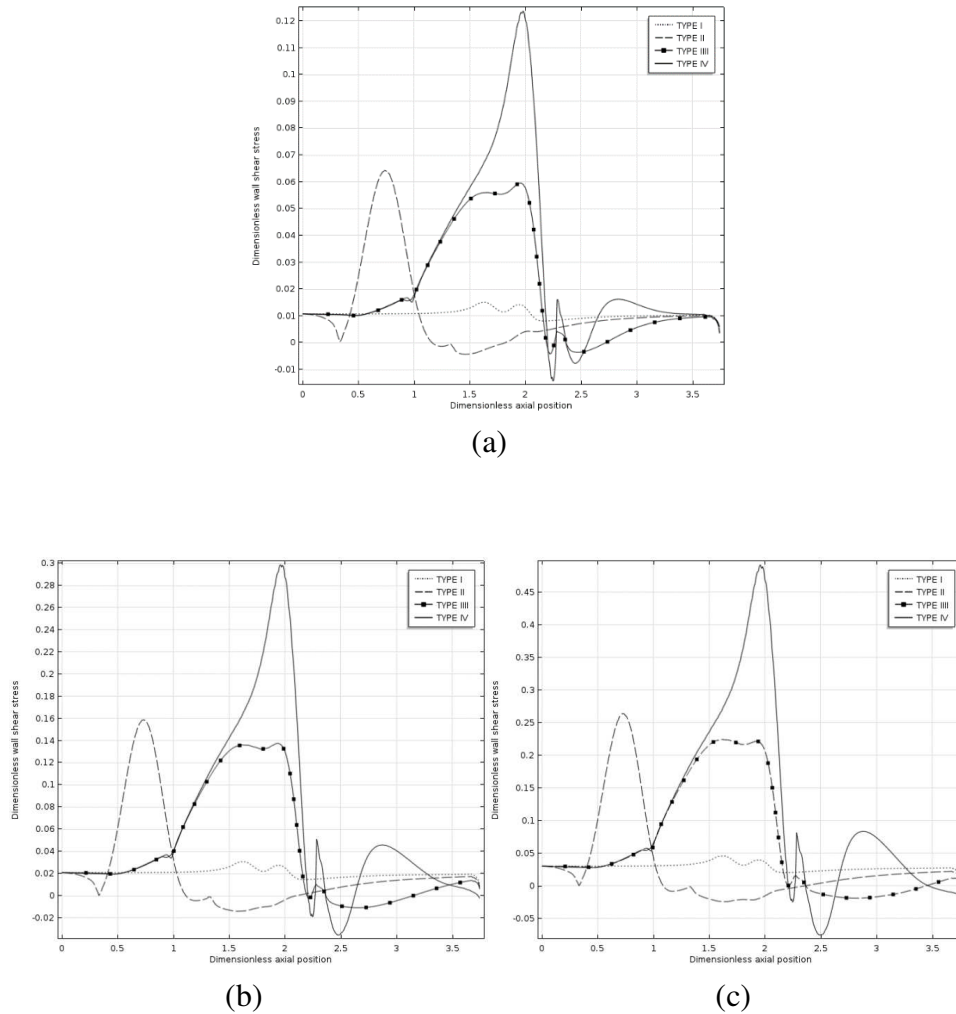(b)   (c)

Figure 7: Wall Shear Stress distributions for different TYPE of model geometries and blood rheology

the effect of stenosis locations on the flow parameters of velocity are investigated not only along the stenotic region, but also on the daughter artery. The flow velocity is considerably influenced by the varying locations of stenosis. Also, the development of flow stagnation and reversal may promote the worsening effects of cardiovascular disease, which is the thrombosis occurrence. In the future, we would like to incorporate time and other haemodynamic effects to further study and discuss.

Acknowledgments

References

[1] Zaman, A., Ali, N., Sajid, M. and Hayat, T. Effects of Unsteadiness and non-Newtonian Rheology on Blood Flow through a Tapered Time-Variant Stenotic Artery. *AIP Advances*. 2015. 5(3): 0371291- 03712913.

[2] Kumar, D. B., Satyanarayana, R. K., Sanjeev, K., and Narendra D. Application of Heat source and chemical reaction in MHD blood flow through permeable bifurcated arteries with inclined magnetic field in tumor treatments. *Results in Applied Mathematics*. 2021. 10: 100151.

[3] Rabby, M. G., Shupti, S. P. and Molla, M. M. Pulsatile Non-Newtonian Laminar Blood Flows through ArterialDouble Stenoses. *Journal of Fluids*. 2014. 2014(757902): 1-13.

[4] Abdelwahab, A. M., Mekheimer, Kh S., Khalid K. A., EL-Kholy, A. and Sweed, N. S. Numerical simulation of electroosmotic force on micropolar pulsatile bloodstream through aneurysm and stenosis of carotid. *Waves in Random and Complex Media*. 2021. 1-32.

[5] Iakovou, I., Ge, L. and Colombo, A. Contemporary Stent Treatment of Coronary Bifurcations. *Journal of the American College of Cardiology*. 2005. 46: 1447-1455.

[6] Lefèvre, T., Louvard, Y. and Morice, M. C. Stenting of Bifurcation Lesions: Classification, Treatments, and Results. *Catheterization and Cardiovascular Interventions*. 2000. 49: 274–283 (2000).

[7] Pan, M., Medina, A. and Lezo, J. S. Coronary Bifurcation Lesions Treated with Simple Approach (from the Cordoba & Las Palmas [CORPAL] Kiss Trial). *Am J Cardiol*. 2011. 107: 1460 –1465.

[8] Medina, A., Lezo, J. S. and Pan, M. A new classification of coronary bifurcation lesions. *Rev Esp Cardiol*. 2006. 59: 183–184.

[9] Peacock, J., Hankins, S., Jones T. and Lutz, R. Flow instabilities induced by coronary artery stents: assessment with an in vitro pulse duplicator. *Journal of biomechanics*. 1995. 28(1): 17-26.

[10] Nicoud, F., Vernhet, H. and Dauzat, M. A numerical assessment of wall shear stress changes after endovascular stenting. *Journal of biomechanics*. 2005. 38(10): 2019-2027.

[11] Zarandi, M. M., Mongrain R. and Bertrand, O.F. Non-Newtonian Hemodynamics and Shear Stress Distribution in Three-Dimensional Model of Healthy and Stented Coronary Artery Bifurcation. In *Proceeding of the COMSOL Conference-2010*. 2010.

[12] Pedley, T. J. *The Fluid Mechanics of Large Blood Vessel*. Cambridge University Press. 1980.

[13] Berger S. A. and Jou, L. D. Flows in Stenotic Vessels. *Annual Review of Fluid Mechanics*. 2000. 32(1): 347-382.

[14] Johnston, B. M., Johnston, P., Corney, S. and Kilpatrick, D. Non-NewtonianBlood Flow in Human Right Coronary Arteries: Steady State Simulations. *Journal of Biomechanics*. 2004. 37(5): 709-720.

[15] Dubey, A. B., Vasu, O., Anwar, B. and Gorla, R. S. R. Finite element computation of magneto-hemodynamic flow and heat transfer in a bifurcated artery with saccular aneurysm using the Carreau-Yasuda biorheological model. *Microvascular Research*. 2021. 138: 104221.

[16] Johnston, B. M., Johnston, P., Corney, S. and Kilpatrick, D. Non-Newtonian Blood Flow in Human Right Coronary Arteries: Transient Simulations. *Journal of Biomechanics*. 2006. 39(6): 1116-1128.

[17] Achab, L., Mahfoud, M. and Benhadid S. Numerical Study of The Non-Newtonian Blood Flow in a Stenosed Artery Using Two Rheological Models. *THERMAL SCIENCE.* 2016. 20(2): 449-460.

[18] Bakheet, A., Alnussairy, E., Ismail, Z. and Amin, N. Blood Flow Through An Inclined Stenosed Artery. *Applied Mathematical Sciences.* 2016. 10: 235-254.

[19] Mandal, P. K., Chakravarty, S. and Mandal, A. Numerical Study of The Unsteady Flow of Non-Newtonian Fluid through Differently Shaped Arteria Stenoses. *International Journal of Computer Mathematics*. 2007. 84(7): 1059-1077.

[20] Sarifuddin., Chakravarty, S. and Mandal, P. K. Effect of Asymmetry and Roughness of Stenosis on Non-Newtonian Flow Past an Arterial Segment. *International Journal of Computational Methods*. 2009. 6(3): 361-388.

[21] Bakheet, A., Alnussairy, E., Ismail, Z. and Amin, N. Generalized Power-Law Model of Magnetohydrodynamic Blood Flow with Heat Transfer. *Indian Journal of Public Health Research & DevelopmentI*. 2018. 9(2): 794-800.

[22] Yao, H., Ang, K. C., Yeo, J. H. and Sim, E. K. W. Computational Modelling of Blood Flow through Curved Stenosed Arteries. *Journal of medical engineering & technology*. 2000. 24(4): 163-168.